Article ID: 1000-324X(2022)04-0445-07 **DOI:** 10.15541/jim20210270

Reversible Conversion between Space-confined Lead Ions and Perovskite Nanocrystals for Confidential Information Storage

ZHANG Guoqing[1,2], QIN Peng[1], HUANG Fuqiang[1,2,3]

(1. State Key Laboratory of High Performance Ceramics and Superfine Microstructure, Shanghai Institute of Ceramics, Chinese Academy of Sciences, Shanghai 200050, China; 2. School of Physical Science and Technology, ShanghaiTech University, Shanghai 201210, China; 3. State Key Laboratory of Rare Earth Materials Chemistry and Applications, College of Chemistry and Molecular Engineering, Peking University, Beijing 100871, China)

Abstract: Luminescent materials have been widely used in confidential information protection and anticounterfeiting. Luminescent lead halide perovskite nanocrystals, which can be converted from the lead source through a two-step method, are attractive candidates for information encryption and decryption. Herein, the reversible conversion between the invisible lead-organic framework and the luminescent $MAPbBr_3$ nanocrystals is achieved, together with their further application on information storage by inkjet printing technology. The lead ions are embedded into the metal-organic frameworks through coordination with the 2-methylimidazole linkers. The inherent confined distribution of lead ions facilitates the *in-situ* growth of perovskite nanocrystals in the second step without the assistance of external bulky ligands. The recorded information was firstly encrypted by the lead organic frameworks, which is invisible under ambient and UV light. After reacting with methylammonium bromide, the perovskite nanocrystals are *in-situ* formed, and the information becomes readable under UV light. Using methylammonium bromide and water as the decryption and encryption reagents could also switch on/off the luminescence, therefore, realizing the confidential information storage.

Key words: perovskite nanocrystal; photoluminescence; inkjet printing; information storage

Nowadays information security plays more and more important roles in the military and economic fields. Among various information protection technologies, the stimuli-responsive luminescence has attracted lots of attention due to low cost and ease of fabrication. Initially, transparent fluorescent materials were directly employed for the confidential information encryption, and the decryption was completed according to the luminescent response of these materials under external stimuli (humidity, temperature and UV light). In addition to relying on those facile signal "switch on-off" determinations, higher-security encryptions were achieved through multimode emission integrated in one single ink[1-3], luminescence lifetime-dependent emission[4-6] and emission intensity-based decoding[7-8]. However, these elaborate emission inks complicate the whole fabrication process and increase the cost of preparation. Besides, the specific equipment is required to decrypt the encoding data, which is certainly inconvenient for the practical applications[9]. Accordingly, the exploration of novel luminescent inks possessing cost advantage and competitive performance are alternatively desirable for the efficient anti-counterfeiting purposes.

Recently, the organic-inorganic hybrid perovskites have emerged as effective photoluminescence materials due to high photoluminescence quantum yields, narrow emission bands and tunable emission spectra[10]. Moreover, the soft ionic structure, low formation energy, together with the low cost facilitate their usage as smart luminescent materials. By space-confining the $CsPbBr_3$ nanocrystals into porous silica matrix, the reversible conversion between luminescent $CsPbBr_3$ and non-luminescent $CsPb_2Br_5$ phase can be achieved by using water as the external stimuli. The printed information can be hidden and recovered through moisture treatment and evaporation, res-

Received date: 2021-04-26; **Revised date:** 2021-06-29; **Published online:** 2021-07-20
Foundation item: National Natural Science Foundation of China (21871008, 51872315); Key Research Program of Frontier Science, Chinese Academy of Sciences (QYZDJ-SSW-JSC013)
Biography: ZHANG Guoqing (1992–), male, PhD candidate. E-mail: zgq201209@foxmail.com
张国庆(1992–), 男, 博士研究生. E-mail: zgq201209@foxmail.com
Corresponding author: QIN Peng, associate professor. E-mail: qinpeng@mail.sic.ac.cn;
HUANG Fuqiang, professor. E-mail: huangfq@mail. sic.ac.cn
秦 鹏, 副研究员. E-mail: qinpeng@mail.sic.ac.cn; 黄富强, 研究员. E-mail: huangfq@mail.sic.ac.cn

pectively[11]. Besides phase transition, Huang, *et al*.[12-13] reported the *in-situ* formation and decomposition of luminescent $CsPbX_3$ quantum dots within transparent glasses through femtosecond laser irradiation and thermal treatment, realizing the reversible information writing and erasing. Another attractive technique to realize the information protection and storage was developed by firstly constructing an invisible lead-based metal-organic frameworks and then converting the lead ions to luminescent perovskite nanocrystals with a two-step method. The photoluminescence can be quenched and recovered through solvent impregnation and halide salt conversion. With this strategy, the reversible on/off switching of photoluminescence for information encryption and decryption could be realized under ambient conditions[14].

Herein, we utilize the strong interaction between 2-methylimidazole and lead ions to construct a novel space-confined lead framework (Pb-ZIF). The unique distribution of lead ions within the framework facilitates the *in-situ* growth of perovskite nanocrystals after reacting with MABr (MA=CH_3NH_3). The obtained $MAPbBr_3$ NCs@Pb-ZIF exhibits bright luminescence under UV excitation. The recorded information was firstly encrypted by printing the Pb-ZIF ink on parchment paper, which is invisible under ambient and UV light. The subsequent MABr solution spray initializes the *in-situ* growth of perovskite nanocrystals, making the encrypted information readable under UV light. Using methylammonium bromide and water as the decryption and encryption reagents could switch on/off the luminescence. Different from the direct printing of perovskite nanocrystals, this two-step strategy by separating the confidential information recording and displaying provides the information protection with a higher level.

1 Experimental

1.1 Sample preparation

Pb-ZIF powder was synthesized using a similar modified procedure reported by Sadeghzadeh[15]. Specifically, 6 mmol 2-methylimidazole (Aladdin, 98%) was ultrasonicaly dissolved in 50 mL deionized water (termed as solution A), and then 0.05 mol·L^{-1} (20 mL) $Pb(NO_3)_2$ (Adamas, 99%) aqueous solution (solution B) was dropwise slowly added into solution A. A kind of clear and transparent solution C was obtained. Finally, an appropriate amount of ethanol (200 mL) was swiftly poured into the above solution C to precipitate Pb-ZIF powders. The obtained powder was rinsed three times with ethanol and then dried at 60 ℃ for further use. For the synthesis of $MAPbBr_3$ NCs@Pb-ZIF powder (similar to the conversion process reported by Zhang[14]), 100 mg Pb-ZIF powder was dispersed in 10 mL *n*-hexane (Greagent, ≥97%) under constant stirring (termed as suspension D). Then the predissolved MABr (Greatcell Solar) butanol solution (1.5 mL, 20 mg/mL) was rapidly injected, and the white suspension D immediately turned into green emissive suspension E. The as-formed precipitate was then collected and dried (60 ℃) into powder for further characterizations.

1.2 Information coding-decoding procedure

The invisible transparent ink consisting of 1.99 g $Pb(NO_3)_2$, 1.48 g 2-methylimidazole and 10 mL *N*,*N*-dimethylformamide (DMF , Sigma Aldrich, 99.8%) was loaded into the ink printer (Canon, PIXMA iP2780), and the predesigned various patterns were printed directly on the commercial available paper. Considering the limited amounts of solvent used for each printing procedure, the obtained coding information can be immediately implemented for decoding process. Similar to the conversion process of luminescent $MAPbBr_3$ NCs@Pb-ZIF powders, the spray of MABr butanol solution (20 mg/mL) was employed to realize the *in-situ* formation of $MAPbBr_3$ NCs at the place where information was recorded.

1.3 Characterization

X-ray diffraction data were collected by using a Bruker D8 Advance powder diffractometer. TEM and corresponding SAED analyses were performed by using JEM-2100F microscope. SEM images and EDS mappings were conducted on JEOL 7800F microscope. Absorption spectra were determined by a Hitachi U-4100 UV-Vis spectrometer. Fluorescence spectrometer (Fluorolog, HORIBA FL-3) was used to record the PL and PL decay curves of the samples. The chemical nature of the powders was investigated by XPS Mg Kα excitation (RBD upgraded PHI-5000C ESCA system, PerkinElmer), the sample of $MAPbBr_3$ NCs@Pb-ZIF was treated with ion etching for 10 s to investigate the internal distribution of the corresponding elements. Thermogravimetric analysis (TGA) was measured on Netzsch STA449F3 instrument (5 ℃/min, under Argon atmosphere).

2 Results and discussion

A new metal-organic framework (Pb-ZIF) was constructed through the chemical bonding between 2-methylimidazole and lead ions. The $MAPbBr_3$ nanocrystals were *in-situ* grown within this framework after reacting with MABr (denoted as $MAPbBr_3$ NCs@Pb-ZIF). The detailed synthesis process was presented in the experimental section. The obtained $MAPbBr_3$ NCs@Pb-ZIF powder exhibits bright green emission under UV excitation (Fig. 1). It is noted that the quantum-confinement is directly realized by the metal-organic framework, without the ad-

dition of bulky ligands or porous matrix. X-ray diffraction (XRD) patterns of Pb-ZIF and $MAPbBr_3$ NCs@Pb-ZIF powders are shown in Fig. S1. Pb-ZIF shows a sharp and intense peak at ~12.5°, demonstrating the highly crystalline nature of the sample which is further confirmed by well-resolved diffraction spots in the selected area electron diffraction (SAED) pattern (Fig. 2(b)). After reacting with MABr, new peaks at 14.9° and 25.9° are observed, corresponding to the (100) and (111) planes of cubic $MAPbBr_3$ ($Pm\bar{3}m$ space group)[16]. The diffraction peaks of $MAPbBr_3$ nanocrystals are much weaker than those of Pb-ZIF, indicating that the second conversion reaction might mainly occur on the surface of the Pb-ZIF framework, and no bulk perovskite are formed. These results also indicate that $MAPbBr_3$ NCs were *in-situ* formed within Pb-ZIF framework, and its formation does not dramatically influence the crystal structure of the matrix. Nonetheless, the decreased main peaks intensity of Pb-ZIF

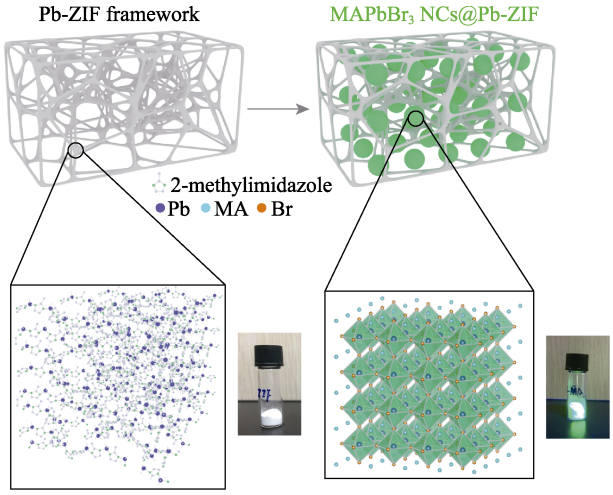

Fig. 1　Schematic diagram of *in-situ* growth of $MAPbBr_3$ NCs from Pb-ZIF framework and optical images of Pb-ZIF (left under ambient light), and $MAPbBr_3$ NCs@Pb-ZIF (right under UV light)

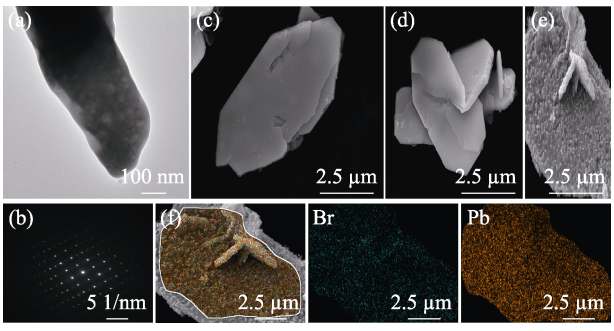

Fig. 2　(a) TEM image and (b) SAED pattern of Pb-ZIF powders SEM images of (c, d) Pb-ZIF and (e) $MAPbBr_3$ NCs@Pb-ZIF powders, and (f) elemental mappings of $MAPbBr_3$ NCs@Pb-ZIF powder

along with unshifted diffraction angle implied the redistribution of electron density in the Pb-ZIF structures[17]. Fig. 2(c, d) show the scanning electron microscopy (SEM) images of the Pb-ZIF, which are well-organized flakes with a thicknesses of ~250 nm. After the conversion reaction, the Pb-ZIF framework preserves the original shape but with the generation of small nanoparticles on its surface (Fig. 2(e)). The elemental mapping of the prepared $MAPbBr_3$ NCs@Pb-ZIF (Fig. 2(f)) shows uniform distribution of elements Br and Pb, which further confirms the *in-situ* formation of the $MAPbBr_3$ perovskite nanocrystals.

X-ray photoelectron spectroscopy (XPS) was conducted to investigate the coordination environment of ions in Pb-ZIF and $MAPbBr_3$ NCs@Pb-ZIF powders. Two new peaks assigned to $Br3d_{5/2}$ and $Br3d_{3/2}$ are observed at 68.3 and 69.0 eV (Fig. 3(a, c))[18], indicating the insertion of Br ions after the reaction with MABr. Meanwhile, in the high-resolution Pb4f XPS spectrum (Fig. 3(b)), two signals corresponding to $Pb4f_{7/2}$ and $Pb4f_{5/2}$ slightly shift to higher binding energy, which suggests that lead ions in $MAPbBr_3$ nanocrystals originate from the Pb-ZIF framework rather than the free Pb ions adsorbe on the surface. No metallic Pb states notorious as carrier trapping centers[19] are detected from high-resolution Pb4f XPS spectrum. It is noted that the loose structure of the Pb-ZIF framework can facilitate the diffusion of MABr and thus promote the conversion of Pb ions encapsulated inside which may account for the evident Br3d signals after ion etching (Fig. 3(d)).

Fig. 4(a) shows the absorption spectra of the Pb-ZIF and $MAPbBr_3$ NCs@Pb-ZIF powders. The absorption of Pb-ZIF is negligible in the whole visible region, while $MAPbBr_3$ NCs@Pb-ZIF possesses a steep absorption edge near 530 nm. The excitonic absorption at 513 nm confirms the strong confinement of perovskite nanocrystals in the $MAPbBr_3$ NCs@Pb-ZIF. Generally the exciton binding energy (E_b) is slightly higher than the thermal energy (RT=26 meV) which results in the domination of free carriers in the $MAPbBr_3$ crystals[20-21]. The notable excitonic feature in this case indicates the strong confinement of the sample. As can be seen from the steady-state photoluminescence (PL) spectrum (Fig. 4(b)), the prepared $MAPbBr_3$ NCs@Pb-ZIF exhibits a sharp and narrow emission at 519 nm with a full width half maximum of only 25 nm under UV excitation. The confinement effect also leads to a blue-shifted PL emission compared with the bulk $MAPbBr_3$ crystals[16]. The PL decay measurement was performed to investigate the recombination kinetics of the $MAPbBr_3$ NCs@Pb-ZIF powder (Fig. 4(c)). With the bi-exponential fitting (Table S1), an average lifetime (τ_{av}) of 6.1 ns composed of trap-assisted recombination lifetime (fast decay component,

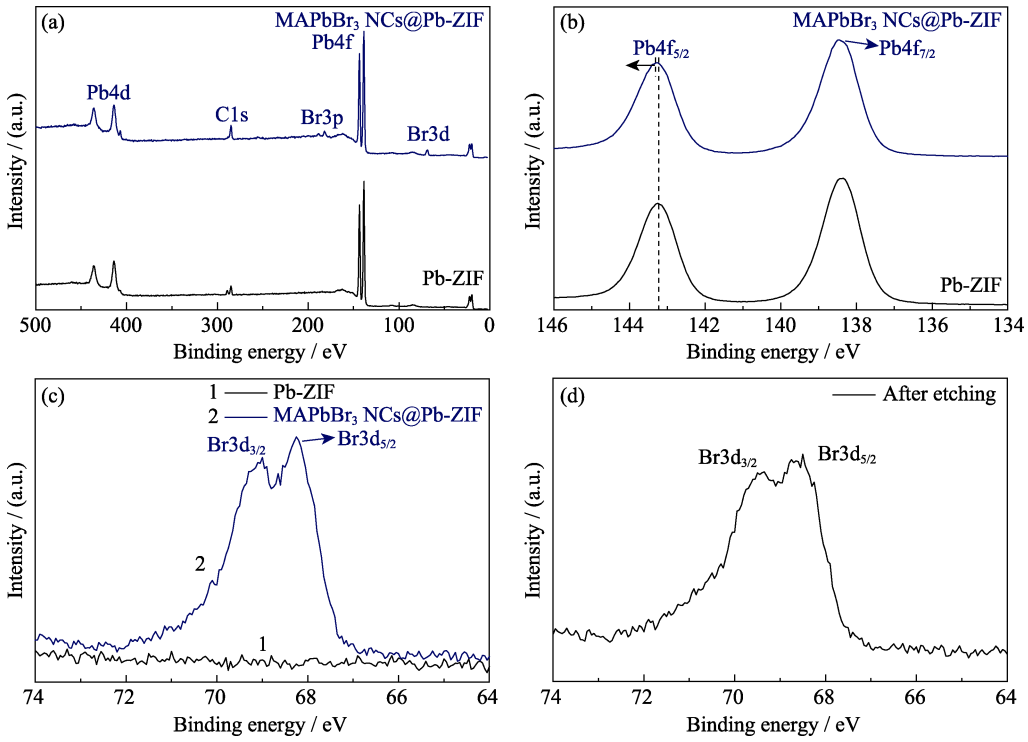

Fig. 3 XPS spectra of Pb-ZIF and $MAPbBr_3$ NCs@Pb-ZIF samples

(a) Survey XPS spectra; (b) Pb4f XPS spectra (The offset of Pb 4f peaks marked by an arrow); (c) Br3d XPS spectra of Pb-ZIF and $MAPbBr_3$ NCs@Pb-ZIF samples; (d) Br3d XPS spectrum of $MAPbBr_3$ NCs@Pb-ZIF sample after etching

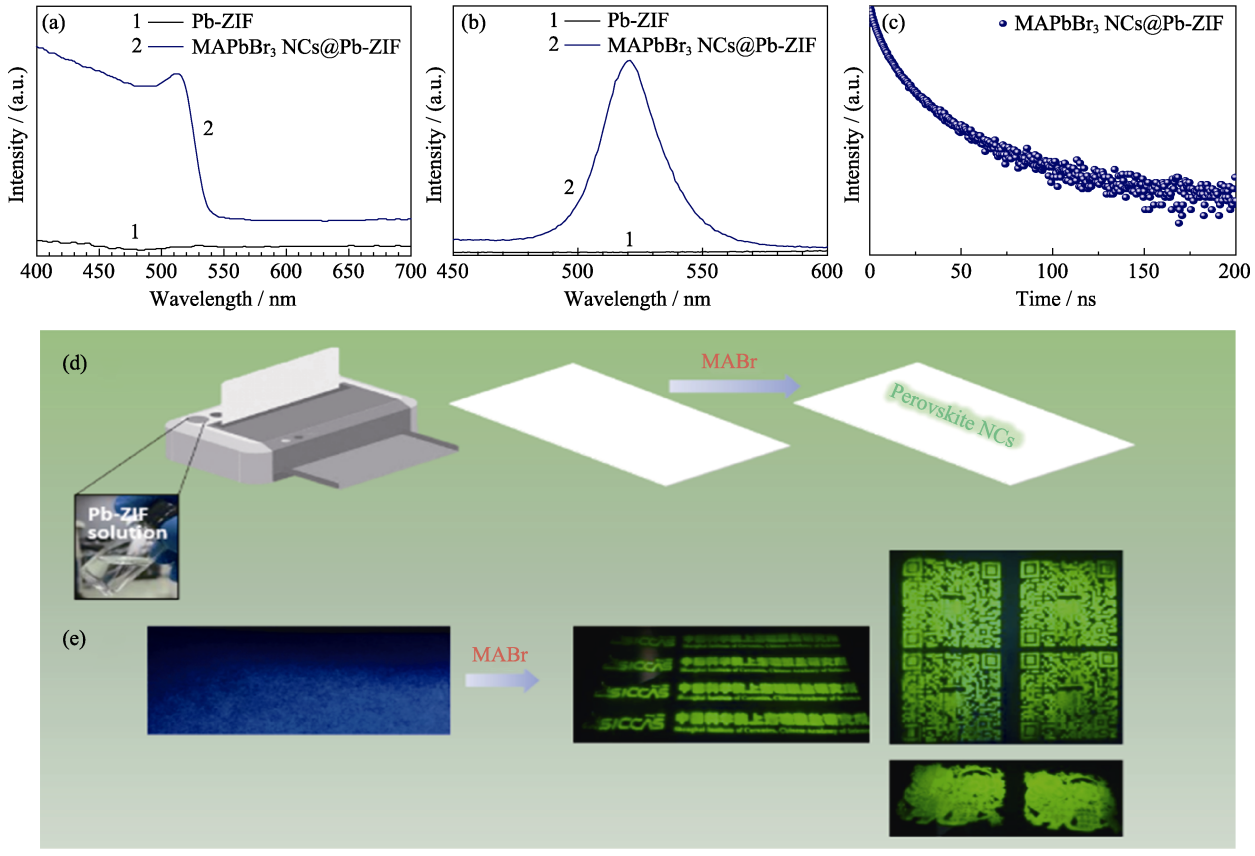

Fig. 4 (a) Absorption and (b) steady-state PL spectra of Pb-ZIF and $MAPbBr_3$ NCs@Pb-ZIF samples; (c) PL decay kinetics of $MAPbBr_3$ NCs@Pb-ZIF sample; (d) Schematic confidential information encryption and decryption process based on Pb-ZIF and $MAPbBr_3$ NCs@Pb-ZIF; (e) Optical images of the printed Pb-ZIF and $MAPbBr_3$ NCs@Pb-ZIF patterns under UV excitation

4 ns) and radiative recombination lifetime (slow decay component, 16.3 ns) was calculated, which is similar to the mesoporous silica confined perovskite phosphor but shorter than the colloidal counterparts[22-23]. Although 2-methylimidazole could act as passivating ligands, the surface or structure defects in the emissive powders still need to be further treated for more efficient radiative recombination, especially within this nanocrystalline regime.

Taking advantage of the invisible feature of the Pb-ZIF intermediate and the strong luminescence of the final perovskite nanocrystals, this two-step strategy shows the potential to be used for information encryption and decryption through simple inkjet printing technology. As shown in Fig. 4(d), the transparent and achromic ink was firstly prepared by dissolving the constituent species, $Pb(NO_3)_2$ and 2-methylimidazole, in polar solvent *N*,*N*-dimethylformamide (DMF). The mass production of the predesigned patterns could be realized *via* inkjet printing. To guarantee efficient adhesion and penetration, the commercial paper with fibrous microstructure (Fig. 5(a)) was utilized as the information carrier. Benefitting from the negligible light response of Pb-ZIF (Fig. 4(a) and Fig. S4(a)), the information deposited on the paper is completely invisible under UV and visible light (Fig. 4(e) and Fig. S4(a)), ensuring that the recorded information is faithfully encrypted. After the spray of MABr solution (in *n*-butanol), the printed Pb-ZIF in the patterned area is locally converted to the luminescent $MAPbBr_3$ nanocrystals. Accordingly, the predesigned information was clearly distinguished. Fig. 4(e) highlights the logo of Shanghai Institute of Ceramics, Chinese Academy of Sciences. Other complex luminescent patterns including QR code, lion dance and the Great Wall are also presented in Fig. 4(e) and Fig. S2, indicating the designability and flexIbility of this strategy.

SEM image (Fig. 5(b)) further reveals that the Pb-ZIF crystals nucleate in the printed areas and are well-distributed on the surface of the substrate. No distinguishable absorption is detected under UV and visible light, providing the encrypted information with a high-level security (Fig. S4(a,b)). After the local conversion to the $MAPbBr_3$ nanocrystals, the printed patterns exhibit strong photoluminescence under UV light (Fig. 4(e)), ensuring that the protected information can be accurately identified. Taking into account the ionic characteristics of the organic-inorganic halide perovskites, the structure could be easily destroyed by polar solvents[24]. As shown in Fig. 5(d), the previously identified QR code no longer emits fluorescence under UV light after the water spray treatment, and thus the information is encrypted. After the water is completely volatilized, the emissive QR code patterns could be regenerated again with the spray of MABr solution. The printed pattern exhibits bright green photoluminescence under UV irradiation (Fig. 5(d)), and the PL intensity maintains 74% of its initial value after five consecutive switching cycles (Fig. 5(e)). In this method, the Pb-ZIF acts as a reservoir of lead source for the circular generation of perovskite nanocrystals, which allows the reversible on/off switching of the photoluminescence

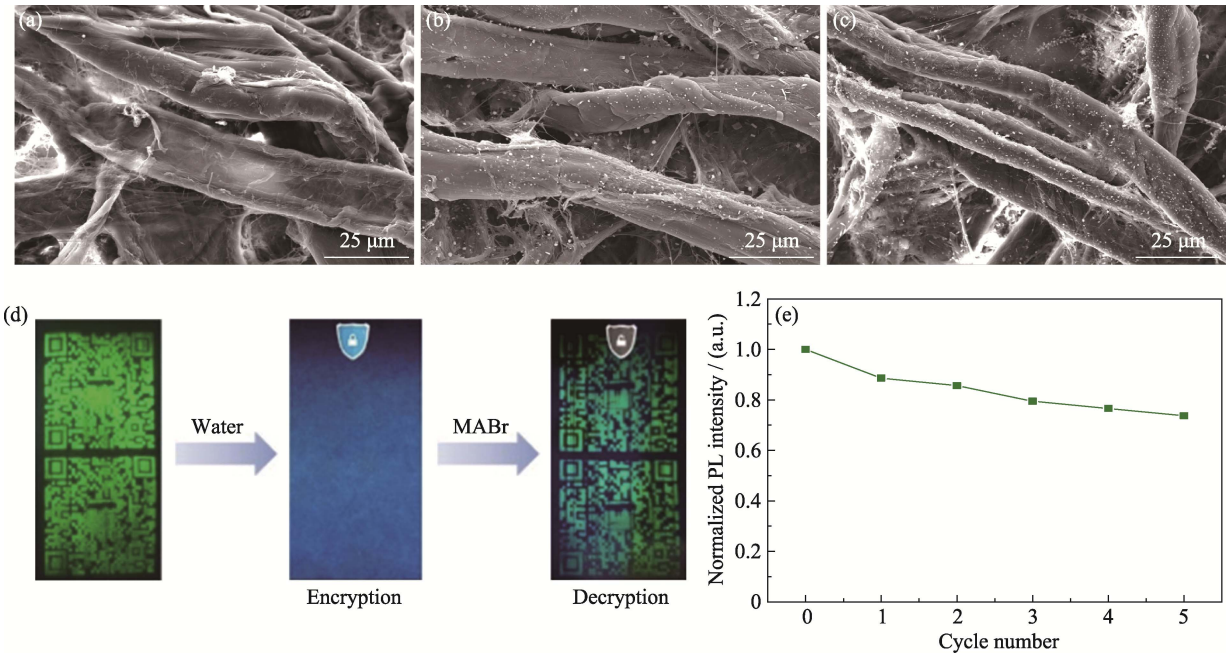

Fig. 5　SEM images of (a) pristine commercial paper, (b) commercial paper after printed with Pb-ZIF ink, (c) commercial paper with $MAPbBr_3$ NCs@Pb-ZIF NCs, (d) representative information encryption and decryption procedure, and (e) PL intensity of the printed $MAPbBr_3$ NCs@Pb-ZIF patterns in the five cycles of encryption and decryption measurement

and realizes the information encryption and decryption. The prepared Pb-ZIF exhibits good thermal stability (Fig. S5), which is beneficial for the practical applications of this system.

3 Conclusion

In conclusion, we have demonstrated the *in-situ* conversion of luminescent perovskite nanocrystals from a novel spaced-confined lead-organic framework, which is constructed through the chemical bonding between lead ions and 2-methylimidazole ligand. The unique distribution of lead ions within the framework facilitates the *in-situ* growth of perovskite nanocrystals after reacting with MABr. This two-step strategy from the invisible intermediate to the photoluminescent nanocrystals is further combined with the inkjet-printing technology to be used for information protection. The invisible Pb-ZIF ink endows the recorded information on parchment paper with a high-security level, and the subsequent MABr solution spray initializes the *in-situ* growth of perovskite nanocrystals, making the encrypted information readable under UV light. The methylammonium bromide and water can be used as the decryption and encryption reagent to switch on/off the luminescence, thus protecting the recorded confidential information.

Supporting materials

Supporting materials related to this article can be found at https://doi.org/10.15541/jim20210270.

References:

[1] GAO Z, HAN Y, WANG F. Cooperative supramolecular polymers with anthracene–endoperoxide photo-switching for fluorescent anti-counterfeiting. *Nature Communications*, 2018, **9:** 3977.

[2] WU W, LIU H, YUAN J, *et al.* Nanoemulsion fluorescence inks for anti-counterfeiting encryption with dual-mode, full-color, long-term stability. *Chemical Communications*, 2021, **57(40):** 4894–4897.

[3] ZHANG Y, HUANG R, LI H, *et al.* Triple-mode emissions with invisible near-infrared after-glow from Cr^{3+}-doped zinc aluminum germanium nanoparticles for advanced anti-counterfeiting applications. *Small*, 2020, **16(35):** 2003121.

[4] DONG H, SUN L D, FENG W, *et al.* Versatile spectral and lifetime multiplexing nanoplatform with excitation orthogonalized upconversion luminescence. *ACS Nano*, 2017, **11(3):** 3289–3297.

[5] LU Y, ZHAO J, ZHANG R, *et al.* Tunable lifetime multiplexing using luminescent nanocrystals. *Nature Photonics*, 2014, **8(1):** 32–36.

[6] ZHOU L, FAN Y, WANG R, *et al.* High-capacity upconversion wavelength and lifetime binary encoding for multiplexed biodetection. *Angewandte Chemie International Edition*, 2018, **57(39):** 12824–12829.

[7] YIN Z, LI H, XU W, *et al.* Local field modulation induced three-order upconversion enhancement: combining surface plasmon effect and photonic crystal effect. *Advanced Materials*, 2016, **28(13):** 2518–2525.

[8] ZHOU D, LIU D, XU W, *et al.* Synergistic upconversion enhancement induced by multiple physical effects and an angle-dependent anticounterfeit application. *Chemistry of Materials*, 2017, **29(16):** 6799–6809.

[9] REN W, LIN G, CLARKE C, *et al.* Optical nanomaterials and enabling technologies for high-security-level anticounterfeiting. *Advanced Materials*, 2020, **32(18):** 1901430.

[10] BERA S, PRADHAN N. Perovskite nanocrystal heterostructures: synthesis, optical properties, and applications. *ACS Energy Letters*, 2020, **5(9):** 2858–2872.

[11] YU X, WU L, YANG D, *et al.* Hydrochromic $CsPbBr_3$ nanocrystals for anti-counterfeiting. *Angewandte Chemie International Edition*, 2020, **59(34):** 14527–14532.

[12] HUANG X, GUO Q, KANG S, *et al.* Three-dimensional laser-assisted patterning of blue-emissive metal halide perovskite nanocrystals inside a glass with switchable photoluminescence. *ACS Nano*, 2020, **14(3):** 3150–3158.

[13] HUANG X, GUO Q, YANG D, *et al.* Reversible 3D laser printing of perovskite quantum dots inside a transparent medium. *Nature Photonics*, 2020, **14(2):** 82–88.

[14] ZHANG C, WANG B, LI W, *et al.* Conversion of invisible metal-organic frameworks to luminescent perovskite nanocrystals for confidential information encryption and decryption. *Nature Communications*, 2017, **8:** 1138.

[15] SADEGHZADEH H, MORSALI A. Sonochemical synthesis and structural characterization of a nano-structure Pb (II) benzentricarboxylate coordination polymer: new precursor to pure phase nanoparticles of Pb (II) oxide. *Journal of Coordination Chemistry*, 2010, **63(4):** 713–720.

[16] SAIDAMINOV M I, ABDELHADY A L, MURALI B, *et al.* High-quality bulk hybrid perovskite single crystals within minutes by inverse temperature crystallization. *Nature Communications*, 2015, **6:** 7586.

[17] SUN J Y, RABOUW F T, YANG X F, *et al.* Facile two-step synthesis of all-inorganic perovskite $CsPbX_3$ (X=Cl, Br, and I) zeolite-Y composite phosphors for potential backlight display application. *Advanced Functional Materials*, 2017, **27(45):** 1704371.

[18] PU Y C, FAN H C, LIU T W, *et al.* Methylamine lead bromide perovskite/protonated graphitic carbon nitride nanocomposites: interfacial charge carrier dynamics and photocatalysis. *Journal of Materials Chemistry A*, 2017, **5(48):** 25438–25449.

[19] JUNG D H, PARK J H, LEE H E, *et al.* Flash-induced ultrafast recrystallization of perovskite for flexible light-emitting diodes. *Nano Energy*, 2019, **61:** 236–244.

[20] BARANOWSKI M, PLOCHOCKA P. Excitons in metal-halide perovskites. *Advanced Energy Materials*, 2020, **10(26):** 1903659.

[21] LI B, LONG R, XIA Y, *et al.* All-inorganic perovskite $CsSnBr_3$ as a thermally stable, free-carrier semiconductor. *Angewandte Chemie International Edition*, 2018, **57(40):** 13154–13158.

[22] MALGRAS V, TOMINAKA S, RYAN J W, *et al.* Observation of quantum confinement in monodisperse methylammonium lead halide perovskite nanocrystals embedded in mesoporous silica. *Journal of the American Chemical Society*, 2016, **138(42):** 13874–13881.

[23] YAN F, XING J, XING G, *et al.* Highly efficient visible colloidal lead-halide perovskite nanocrystal light-emitting diodes. *Nano Letters*, 2018, **18(5):** 3157–3164.

[24] ZHANG C, LI W, LI L. Metal halide perovskite nanocrystals in metal–organic framework host: not merely enhanced stability. *Angewandte Chemie International Edition*, 2021, **60(14):** 7488–7501.

空间限域铅离子与钙钛矿纳米晶间的可逆转换与信息存储应用

张国庆[1,2], 秦　鹏[1], 黄富强[1,2,3]

(1. 中国科学院 上海硅酸盐研究所, 高性能陶瓷和超微结构国家重点实验室, 上海 200050; 2. 上海科技大学 物质科学与技术学院, 上海 201210; 3. 北京大学 化学与分子工程学院, 稀土材料化学及应用国家重点实验室, 北京 100871)

摘　要: 发光材料在机密信息保护与防伪领域中发挥着重要作用。钙钛矿纳米晶作为一类高效低成本发光材料可通过两步法原位转换获得, 使其在信息加密、解密领域极具应用前景。本研究探索了“不可见”铅有机框架和发光 $MAPbBr_3$ 钙钛矿纳米晶间的可逆转换, 以及它们在荧光打印信息存储中的应用。通过铅离子与 2-甲基咪唑配位构建新型金属有机框架, 实现铅离子限域分布, 在此基础上通过与甲胺溴原位反应生成钙钛矿纳米晶。利用金属有机框架在可见/紫外光下无光响应的特性, 通过墨水打印对信息进行加密存储。加密信息经甲胺溴喷雾处理, 引发原位反应生成钙钛矿纳米晶, 在紫外光下表现出强光致发光特性, 实现信息解密。利用甲胺溴和水作为解密和加密试剂可实现荧光的多次循环显示与消除。

关　键　词: 钙钛矿纳米晶; 光致发光; 墨水打印; 信息存储

中图分类号: TQ424　　**文献标志码:** A

Supporting Materials:

Reversible Conversion between Space-confined Lead Ions and Perovskite Nanocrystals for Confidential Information Storage

ZHANG Guoqing[1,2], QIN Peng[1], HUANG Fuqiang[1,2,3]

(1. State Key Laboratory of High Performance Ceramics and Superfine Microstructure, Shanghai Institute of Ceramics, Chinese Academy of Sciences, Shanghai 201210, China; 2. School of Physical Science and Technology, ShanghaiTech University, Shanghai 200031, China; 3. State Key Laboratory of Rare Earth Materials Chemistry and Applications, College of Chemistry and Molecular Engineering, Peking University, Beijing 100871, China)

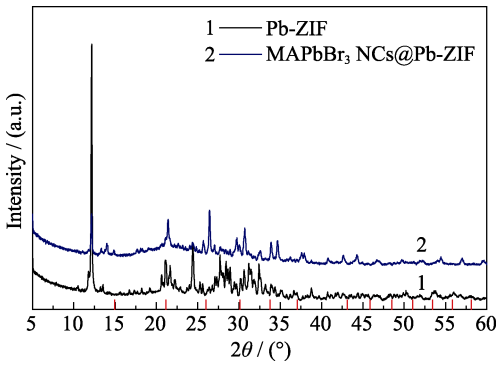

Fig. S1 X-ray diffraction patterns of Pb-ZIF and $MAPbBr_3$ NCs@Pb-ZIF powders
The ideal diffraction peaks of $MAPbBr_3$ were presented as red vertical line

Fig. S2 Additional optical images of the obtained $MAPbBr_3$ NCs@Pb-ZIF patterns on paper under UV excitation

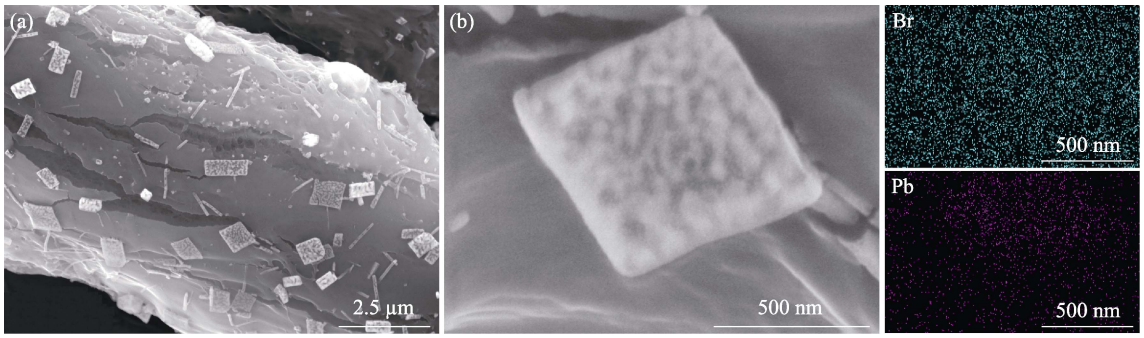

Fig. S3 Enlarged SEM images and corresponding Br and Pb mappings of the commercial paper with $MAPbBr_3$ NCs@Pb-ZIF NCs

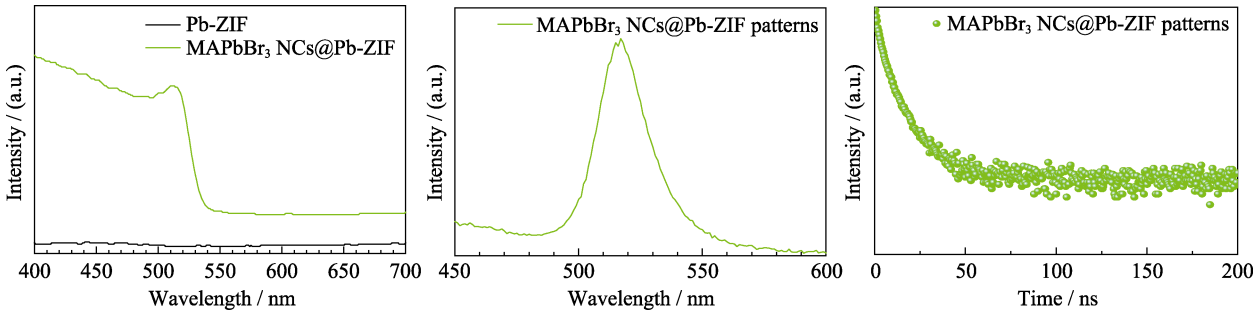

Fig. S4　(a) UV-Vis absorption spectra of the printed Pb-ZIF and $MAPbBr_3$ NCs@Pb-ZIF patterns, (b) steady-state PL spectra and (c) PL decay kinetics of the printed $MAPbBr_3$ NCs@Pb-ZIF patterns

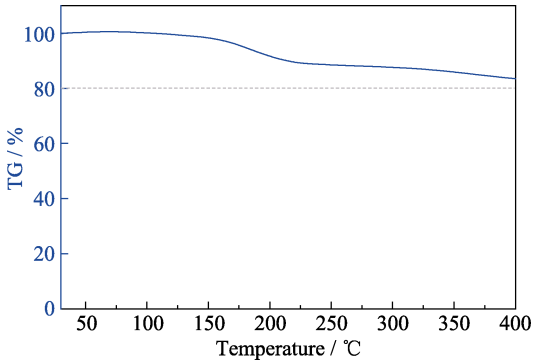

Fig. S5　Thermogravimetric curve of the obtained Pb-ZIF powders

Table S1　PL lifetime for $MAPbBr_3$ NCs@Pb-ZIF powders

	τ_1/ns	f_1	τ_2/ns	f_2	τ_{avg}/ns
Powder	4.0	82.7%	16.3	17.3%	6.1